Modeling of steady-state convective cooling of cylindrical Li-ion cells

K. Shah [a], S.J. Drake [a], D.A. Wetz [b], J.K. Ostanek [c], S.P. Miller [c], J.M. Heinzel [c], A. Jain [a],*

[a] Mechanical and Aerospace Engineering Department, University of Texas at Arlington, USA
[b] Electrical Engineering Department, University of Texas at Arlington, USA
[c] Naval Surface Warfare Center, Carderock Division, U.S. Navy, USA

HIGHLIGHTS

- Presents a new thermal model to predict temperature rise in cylindrical Li-ion cells.
- Results are in excellent agreement with experimental data.
- Results help understand thermal runaway and other thermal issues in Li-ion cells.
- Results predict the importance of various design parameters for thermal performance.
- Results are is used to determine design guidelines for cell sizing.

ARTICLE INFO

ABSTRACT

While Lithium-ion batteries have the potential to serve as an excellent means of energy storage, they suffer from several operational safety concerns. Temperature excursion beyond a specified limit for a Lithium-ion battery triggers a sequence of decomposition and release, which can preclude thermal runaway events and catastrophic failure. To optimize liquid or air-based convective cooling approaches, it is important to accurately model the thermal response of Lithium-ion cells to convective cooling, particularly in high-rate discharge applications where significant heat generation is expected. This paper presents closed-form analytical solutions for the steady-state temperature profile in a convectively cooled cylindrical Lithium-ion cell. These models account for the strongly anisotropic thermal conductivity of cylindrical Lithium-ion batteries due to the spirally wound electrode assembly. Model results are in excellent agreement with experimentally measured temperature rise in a thermal test cell. Results indicate that improvements in radial thermal conductivity and axial convective heat transfer coefficient may result in significant peak temperature reduction. Battery sizing optimization using the analytical model is discussed, indicating the dependence of thermal performance of the cell on its size and aspect ratio. Results presented in this paper may aid in accurate thermal design and thermal management of Lithium-ion batteries.

1. Introduction

A significant amount of research has been carried out in past few decades on Li-ion batteries for energy storage. Despite several advantages over other energy storage technologies such as high specific energy and energy density [1,2], the commercialization of Li-ion battery technology has been slower than expected due to

risks associated with high temperature operation and other safety-related concerns. Such concerns have been highlighted in several recent incidents where Li-ion batteries and battery packs have been found to be responsible for fire aboard aircraft [3,4]. These incidents underscore the importance of developing a fundamental understanding of thermal characteristics of Li-ion cells, particularly the capability of temperature prediction during the operation of a cell.

Similar to any other energy storage device, charging or discharging a Li-ion battery results in heat generation and thus increase in temperature due to exothermic electrochemical reactions and Joule heating [5,6]. Heat generation rate is known to be a function of depth-of-discharge, temperature and the rate at which a cell is charged or discharged, often referred to as C-rate [7].

* Corresponding author. 500 W First St, Rm 211, Arlington, TX 76019, USA. Tel.: +1 817 272 9338; fax: +1 817 272 2952.
E-mail address: jaina@uta.edu (A. Jain).

There are severe limitations to temperature rise permitted in a Li-ion cell, particularly for military applications with high reliability requirements. Thermal runaway at high temperature is a well-known problem in Li-ion batteries [8,9]. While a small temperature rise is known to actually improve performance due to reduced impedance [10], larger temperature rise results in a series of exothermic mechanisms including decomposition of the Solid-Electrolyte Interface (SEI) [11,12] and short circuit due to separator layer rupture from dendrite formation, which ultimately leads to catastrophic failure [8]. As a result, Li-ion cells must operate in a very narrow temperature window. In addition to absolute temperature rise, spatial uniformity of the temperature field is also desirable [13], since this prevents imbalance of temperature-dependent electrochemical reaction rates within the cell or battery pack.

Despite the clear importance of thermal management of cylindrical Li-ion batteries, only a limited amount of literature is available on thermal management and cooling of Li-ion batteries. Only a few studies have reported measurement of thermophysical properties such as thermal conductivity and heat capacity of Li-ion cells [12,14]. Early work in this direction did not recognize the strong anisotropy in thermal conduction in a Li-ion cell. Recent measurements have reported a method for rapid measurement of anisotropic thermal conductivity as well as heat capacity of a Li-ion cell [14]. These measurements indicate nearly two orders of magnitude difference in the radial and axial thermal conductivities of a Li-ion cell [14]. At the battery pack level, some work has been reported on thermal simulations of cooling strategies for Li-ion cells [15,16]. The use of solid-to-liquid phase change materials embedded around cells in a battery pack [17], as well as two-phase flow interstitially within the cell [18] has been proposed for absorbing heat and reducing peak temperature rise. However, such an approach leads to reduced energy density since the phase change material does not store electrochemical energy and results in more complicated cell design. It is important to determine the limits of air/liquid based convective cooling approaches [7] and to develop a sound theoretical framework to understand the dependence of temperature rise in a convectively cooled Li-ion cell on various parameters, such as geometry, cooling parameters, etc. A first step towards effective thermal management of Li-ion cells is the capability to accurately model and predict temperature fields within an operating cell. The temperature field resulting from the heat generation depends on a variety of parameters including geometry, material properties, etc. and needs to be modeled accurately. A number of models are available for predicting volumetric heat generation rates as a function of electrical operating parameters of the cell, ranging from very simple, assuming uniform heat generation rate [5] to very sophisticated [9,13]. Some papers also model volumetric heat generation as a space dependent parameter, accounting for Joule heating that occurs primarily at the two current collector tabs, resulting in non-uniformity, particularly at high discharge rates [9]. Heat generation modeling is complicated by the fact that heat generation may vary with time in specific applications if the charge/discharge rate changes [6]. For example, in an electric vehicle, changes in demand on the battery due to vehicle acceleration and other factors may result in the heat generation rate being a function of time.

In contrast to heat generation modeling, limited work has been reported on temperature field prediction [9,19–24], which is a more critical parameter for safety and performance considerations. While these models provide a basis for temperature prediction, there are several shortcomings. Many past models are one-dimensional [20] and do not account for the spirally-wound geometry of a cylindrical Li-ion cell, boundary conditions encountered in realistic applications, or the thermal conduction anisotropy

in a cylindrical cell. Several thermal models of a Li-ion cell reported in the recent past treat the cell as a lumped body with a single temperature [20,21], which may not be an appropriate assumption for most applications. Three-dimensional thermal models for a Li-ion cell have been presented [22], but this model is solved numerically, and does not offer analytical, closed-form solutions for the temperature field. Some recent work accounts for the spiral nature of the electrodes in a cylindrical Li-ion cell [25], but this work neglects the axial dimension of the cell and does not present a closed-form analytical solution. Recent work has presented analytical models for temperature distribution in prismatic Li-ion cells [23,24] but these models do not readily apply to a cylindrical geometry where heat transfer characteristics are fundamentally different from a prismatic cell.

This paper presents a cell-level, steady-state analytical thermal model of a cylindrical Li-ion cell being cooled on the outside surface by convective flow. Thermal conduction anisotropy within the cell is accounted for. Closed-form analytical solutions for both uniform and space-dependent heat generation rates are presented. The next two Sections present the analytical models, including assumptions, governing equations and closed-form solutions for the temperature field. These models are validated by comparison with experimental measurements on a thermal test cell in Section 4. Section 5 discusses a number of applications of these thermal models including thermal optimization of the convective cooling process and battery sizing. Fundamental limitations of thermal management based on convective cooling are discussed.

2. Analytical model: uniform heat generation

Consider a cylindrical Lithium-ion cell of radius R and height H shown schematically in Fig. 1. Volumetric heat generation rate Q is assumed within the cell due to electrochemical reactions and Joule heating. In this Section, Q is assumed to be spatially uniform, whereas Section 3 considers the case where Q may be a function of space. It is assumed that the outside surfaces of the cell are being cooled with heat transfer coefficients of h_r and h_z for the curved surface and the end surfaces respectively. In case one particular surface is insulated, the respective heat transfer coefficient can be set to zero. Such a situation may arise, for example when the
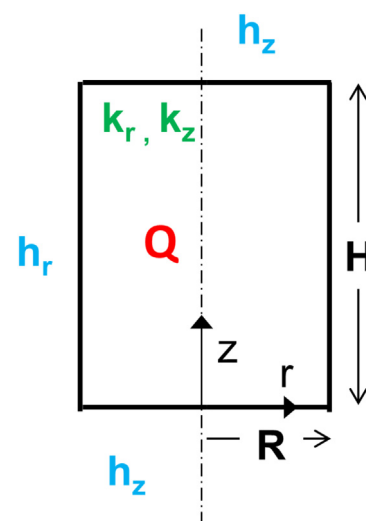

Fig. 1. Schematic diagram showing battery geometry and thermal parameters for the analytical thermal model. Q may be uniform (Section 2) or may vary radially/axially (Section 3).

electrical interface at the anode and cathode ends results in negligible heat loss through the surfaces at $z = 0$ and $z = H$. The ambient temperature for convective cooling is assumed to be T_0. The thermal conductivities in radial and axial directions are assumed to be k_r and k_z respectively. Recent measurements show that k_r and k_z differ by nearly two orders of magnitude [14], thereby indicating the importance of anisotropic modeling of thermal conductivity in a cylindrical Li-ion cell. The governing steady state energy conservation equation in this case is given by

$$\frac{k_r}{r} \frac{\partial}{\partial r} \left(r \frac{\partial \theta}{\partial r} \right) + k_z \frac{\partial^2 \theta}{\partial z^2} + Q = 0 \tag{1}$$

where $\theta(r, z)$ is the temperature rise above ambient, given by

$$\theta(r, z) = T(r, z) - T_0 \tag{2}$$

Equation (1) is a non-homogeneous partial differential equation subject to four homogeneous boundary conditions given by

$$\frac{\partial \theta}{\partial z} = \frac{h_z}{k_z} \theta \quad \text{at } z = 0 \tag{3}$$

$$\frac{\partial \theta}{\partial z} = -\frac{h_z}{k_z} \theta \quad \text{at } z = H \tag{4}$$

$$\frac{\partial \theta}{\partial r} = 0 \quad \text{at } r = 0 \tag{5}$$

$$\frac{\partial \theta}{\partial r} = -\frac{h_r}{k_r} \theta \quad \text{at } r = R \tag{6}$$

The boundary condition in Equation (5) represents the requirement of symmetry and finiteness of the temperature profile at $r = 0$, whereas boundary conditions in Equations (3), (4) and (6) represent energy balance at the respective surfaces.

Briefly, the approach for deriving the solution to Equations (1)–(6) is as follows: The solution is first split into two parts. The first part, which is assumed to be a function of z alone, absorbs the heat generation term, and can be solved by direct integration since it is an ordinary differential equation with two well-defined boundary conditions at $z = 0$ and $z = H$. The second part of the solution, which is a function of both r and z, has three homogeneous boundary conditions and one non-homogeneous boundary condition at $r = R$. The second part of the solution is determined using the separation of variables technique [26]. To do so, the axial eigenvalues μ_n are derived from the homogeneous boundary conditions in z direction. Radial eigenvalues λ_n are related to μ_n through the thermal conductivity ratio [26]. Finally, the co-efficients for the second part of the solution are determined using the non-homogeneous boundary conditions. Details about this solution procedure may be found in Refs. [26–28].

The final solution is given by

$$\theta(r, z) = s(z) + w(r, z) \tag{7}$$

where

$$s(z) = \frac{QH^2}{2k_z} \left[\frac{z}{H} \left(1 - \frac{z}{H} \right) + \frac{1}{Bi_H} \right] \tag{8}$$

and

$$w(r, z) = \sum_{n=1}^{\infty} A_n I_0(\lambda_n r) [\mu_n H \cos(\mu_n z) + Bi_H \sin(\mu_n z)] \tag{9}$$

Here,

$$A_n = \frac{-Bi_R \cdot \frac{1}{H} \int_0^H s(z) [\mu_n H Cos(\mu_n z) + Bi_H Sin(\mu_n z)] \mathrm{d}z}{\frac{1}{2} \left[(\mu_n H)^2 + Bi_H^2 + 2Bi_H \right] \left[\lambda_n R \cdot I_0'(\lambda_n R) + Bi_R I_0(\lambda_n R) \right]} \tag{10}$$

The eigenvalues μ_n are obtained from roots of the transcendental equation

$$\mathrm{Tan}(\mu H) = \frac{2Bi_H \cdot (\mu H)}{(\mu H)^2 - Bi_H^2} \tag{11}$$

where Bi_H and Bi_R are axial and radial Biot numbers, respectively, defined as $Bi_H = h_z H / k_z$ and $Bi_R = h_r R / k_r$.

Finally,

$$\lambda_n = \sqrt{\gamma} \cdot \mu_n \tag{12}$$

where γ is the degree of anisotropy given by

$$\gamma = \frac{k_z}{k_r} \tag{13}$$

For the case of Li-ion batteries, γ is expected to be greater than one. Recent measurements indicate a value of γ around 200 for 26650 geometry LiFePO$_4$ cells [14].

Equations (7)–(13) show that temperature rise at any point in the cell is a function of four non-dimensional parameters — Bi_H, Bi_R, γ, and $QH^2 / 2k_z$.

In addition to the peak temperature rise, another important thermal parameter of interest is the temperature gradient within the cell, defined as the difference between the maximum and minimum temperature. In particular, it is desirable to reduce the difference between maximum and minimum temperature in a cell, since such a gradient leads to performance imbalance, etc. From Equation (7), the temperature gradient within the cell is given by

$$\theta_g \equiv \theta_{\max} - \theta_{\min} = \frac{QH^2}{8k_z} + \sum_{n=1}^{\infty} A_n \left(\mu_n H \cos \left(\frac{\mu_n H}{2} \right) \right. $$
$$\left. + Bi_H \sin \left(\frac{\mu_n H}{2} \right) - \mu_n H \cdot I_0(\lambda_n R) \right) \tag{14}$$

Equation (14) provides a means to quantify the temperature non-uniformity within the cell as a function of various non-dimensional parameters.

One special case of the general solution shown in Equation (7) is of particular interest in the cooling of Li-ion cells. A limiting case for the temperature field is one where there is no convective heat transfer at the axial ends, and all of the heat dissipation occurs at the radial surface. In this case, $h_z = 0$ and the temperature field varies only in the radial direction, and is given by

$$\theta(r) = \frac{QR^2}{4k_r} \left[1 - \left(\frac{r}{R} \right)^2 + \frac{2}{Bi_R} \right] \tag{15}$$

In this case, the temperature rise at any location is a function of Bi_R and $QR^2 / 4k_r$. The degree of anisotropy, γ, does not influence the solution since heat flows only in the radial direction, making the axial thermal conductivity unimportant.

Another special case, likely to be of lesser interest for practical applications is where $h_r = 0$, and heat transfer occurs only through

the end surfaces at $z = 0$ and $z = H$. In this case, temperature variation occurs only in the axial direction and is given by

$$\theta(z) = \frac{QH^2}{2k_z}\left[\frac{z}{H}\left(1 - \frac{z}{H}\right) + \frac{1}{Bi_H}\right] \tag{16}$$

The temperature field solution discussed in this section assumes uniform heat generation rate Q. While this is a reasonable assumption for most cases, it is instructive to also derive the temperature solution for a case where heat generation may be a function of space. For example, high electric current discharge through the cell may result in Joule heating occurring primarily in the metal tabs located at the two ends of the cell [9]. This may result in a z-dependent volumetric heat generation rate [9]. This is exacerbated by the fact that Joule heating increases as the square of the electric current, making the axial variation of heat generation even more prominent. Section 3 next presents analytical models for temperature distribution in a Li-ion cell with space-dependent volumetric heat generation.

3. Analytical model: non-uniform heat generation

Since the rate of electrochemical reactions contributes to heat generation, spatial variation in rate of electrochemical reactions may lead to space-dependent Q. In such a case, the temperature field in the Li-ion cell continues to be governed by Equation (1) and boundary conditions (3)–(6), except that the Q term in Equation (1) is a function of space. Two particular cases of interest are considered in this Section: one in which Q is a function of z only, $Q(z)$; and second, in which Q is a function of r only, $Q(r)$.

$$s(z) = -\frac{H^2}{k_z}\sum_{i=0}^{N}\frac{c_i}{(i+1)(i+2)}\left[\left(\frac{z}{H}\right)^{i+2} - \frac{\left(\frac{z}{H} + \frac{1}{Bi_H}\right)(Bi_H + i + 2)H}{2 + Bi_H}\right] \tag{18}$$

Equation (18) above, together with Equations (9)–(13) completely define the temperature field for axially varying heat generation.

3.2. Solution for radially varying heat generation rate

In case the heat generation rate varies in the radial direction, a solution of the temperature field may be derived by first approximating $Q(r)$ with a polynomial expansion,

$$Q(r) = \sum_{i=0}^{N} c_i\left(\frac{r}{R}\right)^i \tag{19}$$

The solution approach for this case is similar to one described in Section 2 following Equation (7). The solution is given by

$$\theta(r,z) = s(r) + \sum_{n=1}^{\infty} A_{1n}J_0(\lambda_n r)\left[\cosh(\mu_n z) + \cosh(\mu_n(H-z))\right.$$
$$\left. + \frac{h_z}{k_z\mu_n}[\sinh(\mu_n z) + \sinh(\mu_n(H-z))]\right] \tag{20}$$

where

$$A_{1n} = \frac{-h_z\int_0^R rs(r)J_0(\lambda_n r)\,\mathrm{d}r}{\frac{J_0^2(\lambda_n R)}{2\lambda_n^2}\left[(\lambda_n R)^2 + \left(\frac{h_r R}{k_r}\right)^2\right]\left[k_z\mu_n\left(\sinh(\mu_n H) + \frac{h_z}{k_z\mu_n}\cosh(\mu_n H)\right) + h_z\left(\cosh(\mu_n H) + \frac{h_z}{k_z\mu_n}\sinh(\mu_n H)\right)\right]} \tag{21}$$

3.1. Solution for axially varying heat generation rate

The solution approach for this case is similar to one described in Section 2 following Equation (7). The temperature field $\theta(r,z)$ is split into two components, $s(z)$ and $w(r,z)$. The solution approach for $w(r,z)$ is identical to previous section, and the final solution is given by Equations (9)–(13). Here, $s(z)$ is obtained by twice integrating $Q(z)$ and using the boundary conditions in Equations (3)–(4) to determine the constants of integration. Any given well-behaved function $Q(z)$ can be approximated by an N-order polynomial as follows [29]:

$$Q(z) = \sum_{i=0}^{N} c_i\left(\frac{z}{H}\right)^i \tag{17}$$

where the coefficients c_i are chosen appropriately to fit the function $Q(z)$.

With such a polynomial approximation for $Q(z)$, the function $s(z)$ is given by

The eigenvalues λ_n are determined from roots of the transcendental equation

$$Bi_R J_0(\lambda_n R) + \lambda_n R J_0'(\lambda_n R) = 0 \tag{22}$$

Note that μ_n are related to λ_n through the degree of anisotropy, given by Equations (12) and (13).

Also, $s(r)$ is given by

$$s(r) = \sum_{i=0}^{N} \frac{c_i R^2}{(i+2)k_r}\left[\frac{1}{Bi_R} + \frac{1}{(i+2)}\left(1 - \left(\frac{r}{R}\right)^{i+2}\right)\right] \tag{23}$$

Equations (20)–(23) define the temperature solution in the case of radially varying heat generation.

The next sections discuss experimental validation of the analytical model, and present a parametric analysis of the dependence of temperature field on various parameters including the degree of anisotropy and external convective cooling coefficient. A
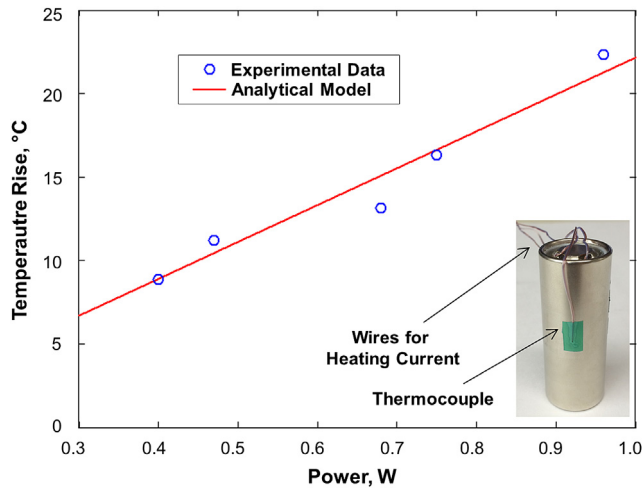
Fig. 2. Comparison of analytical model with experimental data on temperature rise at the outer surface of a 26650 cell at mid-height as a function of heating power.

few design studies enabled by the analytical models are also discussed.

4. Experimental validation

The temperature model presented in this paper is validated by comparison with experimental data. A thermal test cell of the same dimensions as a 26650 cell is fabricated. This test cell has a resistive metal sheet heater rolled up inside. As a result, a desired Joule heating can be produced within the cell by passing an electric current through the sheet heater. A thermocouple is attached at the outer surface at mid-height ($r = R$, $z = H/2$). Steady state temperature measurements are carried out at a number of values of the heating power. Experiments are carried out in natural convection conditions. The analytical model presented in this paper is used to compute the expected temperature at the thermocouple location as a function of heating power. For these computations, thermal properties of the test cell (k_r, k_z) are determined from separate measurements using an adiabatic heating method recently reported by us [14]. A value of $h_r = h_z = 11$ W/m² K is used for the heat transfer coefficient, which is representative of natural convection conditions [30]. Experimental data on temperature rise at different heating powers and analytical model results are both plotted in Fig. 2. The analytical model is in good agreement with experimental
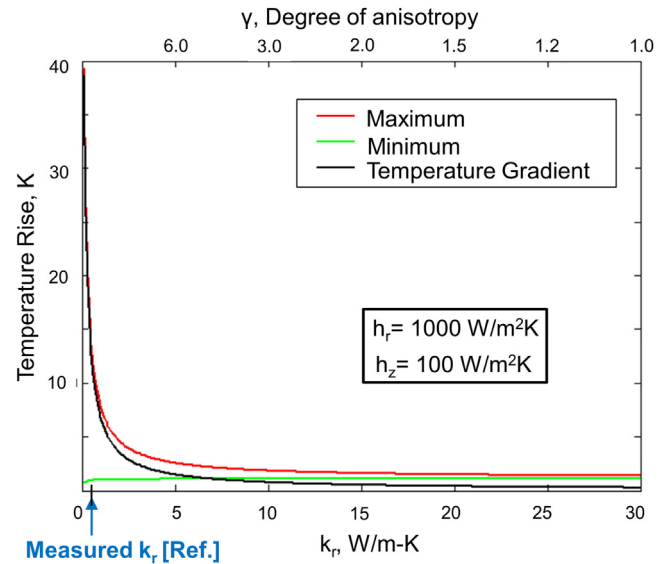

Fig. 4. Variation of peak temperature rise with radial thermal conductivity of battery material, showing significant potential for temperature reduction by improving radial thermal conductivity.

data, and captures the variation of temperature rise as a function of heating power.

In addition, the analytical model presented in this paper is also compared with finite-element model (FEM) simulations. A 26650 cell configuration is considered, with convective heat transfer coefficients of $h_r = 1000$ W/m² K and $h_z = 100$ W/m² K. Recently measured radial and axial thermal conductivity values are used in the model [14]. In each case, the total power dissipated in the 26650 cell is 6 W, which is estimated to correspond to a 10 C (25 A) discharge rate. Fig. 3(a) shows the radial temperature variation at mid-cell height for uniform heat generation of 6 W over the entire cell volume. While the analytical model presented in Section 3.1 accounts for any general polynomial, Fig. 3(b) shows the axial temperature variation at $r = 0$ for two specific cases of z-dependent heat generation rate: a linear variation given by $Q(z) = 2 \cdot Q_{max} z / H$ and a quadratic variation given by $Q(z) = 12 \cdot Q_{max}((z/H) - (1/2))^2$. The coefficients c_i in Equation (17) for the linear and quadratic variations are given by $c_0 = 0$ and $c_1 = 2Q_{max}$; and $c_0 = 3Q_{max}$, $c_1 = -12Q_{max}$, and $c_2 = 12Q_{max}$ respectively. In each case, the analytical model compares well with FEM results.
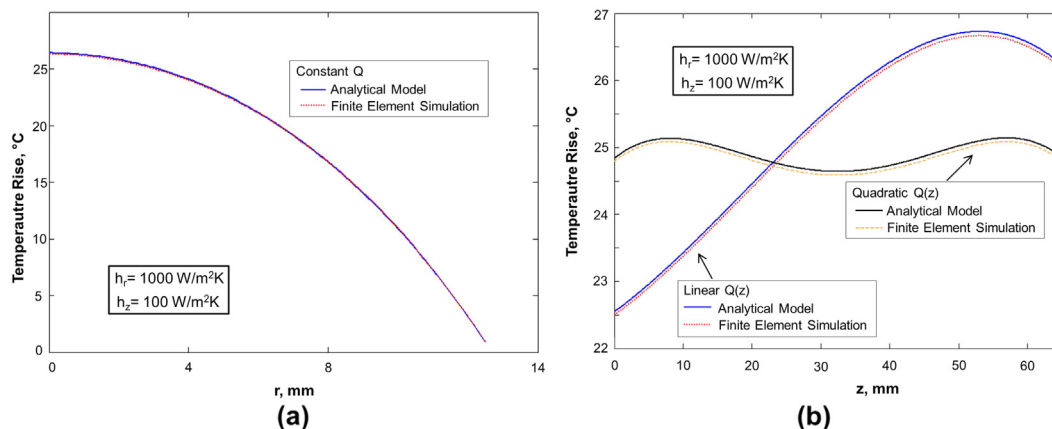

Fig. 3. Comparison of analytical models presented in Sections 2 and 3 with finite-element simulation results for (a) radial temperature variation at $z = H/2$ with uniform heat generation, and (b) axial temperature variation at $r = 0$ with axially varying heat generation.
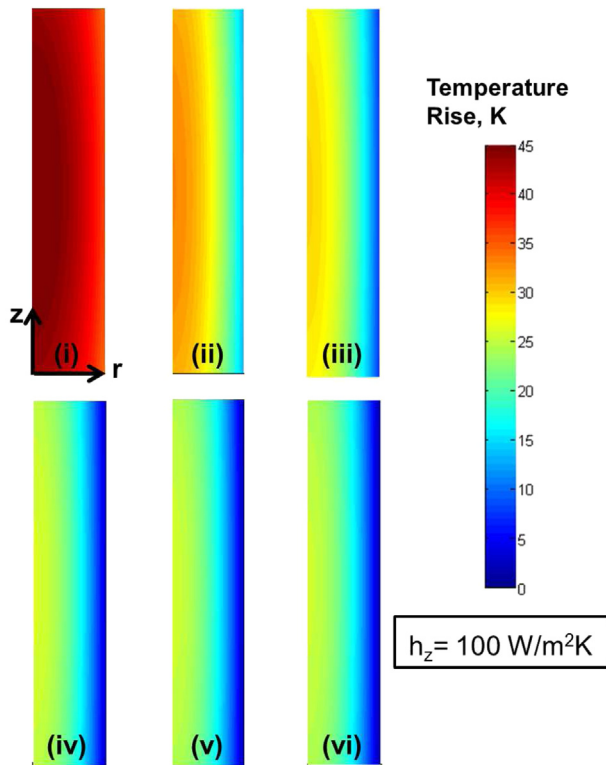
Fig. 5. Variation of temperature field in a 26650 cell as a function of heat transfer coefficient for $h_r =$ (i) 10 W/m^2 K, (ii) 50 W/m^2 K, (iii) 100 W/m^2 K, (iv) 500 W/m^2 K, (v) 1000 W/m^2 K, (vi) 1500 W/m^2 K.

The temperature solution for various cases in Sections 2 and 3 been derived in the form of an infinite series. It is found that these series converge very quickly as the number of terms increases. Considering only three eigenvalues is sufficient for temperature computation with an error of less than 1%.

5. Results and discussion

5.1. Dependence of temperature field on γ and h_r

Fig. 4 plots the peak temperature in the 26650 Li-ion cell generating 6 W heating power as a function of radial thermal conductivity, k_r while other parameters are held constant. Fig. 4 shows a steep increase in peak temperature at low values of k_r. The measured value of k_r [14] is indicated with an arrow on the x-axis. This figure shows that the greater the degree of anisotropy, the larger is the peak temperature rise. There is significant potential for reducing temperature rise by improving radial thermal conductivity and, hence, reducing γ. In effect, radial conduction is the rate-limiting step in heat dissipation. In most practical cases, convective cooling is available at the radial surface at $r = R$, whereas the top and bottom ends are used primarily for electrical interconnection. Finally, since k_z has been measured to be much larger k_r [14], improvement in k_r is more beneficial for temperature reduction.

Fig. 5 shows 2D cross-section temperature color plots for various values of h_r. As the radial convective heat transfer coefficient increases, the cell temperature field reduces as expected. However, beyond approximately $h_r = 1000$ W/m^2 K, there is negligible incremental improvement in the temperature profile. This is further illustrated in Fig. 6(a) which shows temperature line plots as function of r at the cell's mid-height. These results show that

improvement in the external convective heat transfer coefficient helps reduce cell temperature, but this effect quickly saturates. Beyond a specific value, there is not much further improvement. This illustrates the limitation of radial convective cooling mechanisms for cylindrical Li-ion cells. The fundamental reason behind this is that heat flow from within the cell to the ambient encounters two thermal resistances in series — one due to thermal conduction within the cell material, and the second due to convective heat transfer at the outside surface of the cell. In the radial direction, it is the conduction thermal resistance within the cell that is dominant, which is caused by a very low value of radial thermal conductivity [14]. As h_r increases, the convective heat transfer resistance rapidly becomes negligible compared to the conduction resistance, which dominates the thermal response of the cell.

When considering the axial direction, Fig. 6(b) shows the temperature profiles for different values of h_z. As h_z increases, the temperature profiles become lower and lower, and do not saturate similar to the radial case in Fig. 6(a). These results indicate that there may be significant potential in cooling the Li-ion cells from the top and bottom surfaces despite the lower surface area because axial conduction within the cell is more effective than radial conduction. Convective heat transfer at the axial ends may be complicated by the presence of electrical connections. On the other hand, overall heat transfer in the radial direction also requires a close examination of the conduction resistance within the cell, which is shown to be the slower, rate-determining step in radial conduction. Improvements in convective heat transfer at the axial ends, and radial conduction within the cell may be effective technological tools for reducing operating temperature in Li-ion cells.

In addition to absolute temperature rise, temperature gradient within a cell is also of interest for thermal design of cells. It is desirable to minimize spatial variation in temperature within the cell. Temperature variation causes an electrochemical imbalance which may reduce cell lifetime and reliability. Fig. 7 plots the intra-cell temperature gradient as a function of the radial convective heat transfer coefficient h_r. It is found that as h_r improves, the temperature gradient within the cell actually increases. This is because at higher values of h_r, heat generation in the region close to the $r = R$ surface gets dissipated more and more effectively, whereas heat dissipation of heat generated in the core of the cell continues to encounter the internal thermal resistance, which remains unaffected by the improved value of h_r. This demonstrates that while increasing h_r may produce limited improvement in the absolute temperature rise, it may actually increase the intra-cell temperature gradient.

5.2. Battery sizing optimization

One application of the analytical models presented in previous Sections for battery sizing is presented next. Two particular design optimization problems are discussed.

The first problem relates to trade-offs between cell power and temperature rise as functions of cell size. It is of interest to understand how the cell temperature changes as the cell size increases. Fig. 8 plots the total power and temperature rise as functions of the cell radius, assuming that the cell height and other parameters remain constant. Fig. 8 shows that as the cell radius increases and aspect ratio H/R decreases, the power capacity of the cell increases in a quadratic fashion. On the other hand, the peak temperature rise in the cell also increases, but the rate of increase with radius slows down after a certain radius. This is because assuming constant cell power density based on the packing density of the electrode material inside the cell, a larger cell has more storage capacity and hence greater total power. On the other hand, increased size also leads to greater heat generation, which causes greater temperature
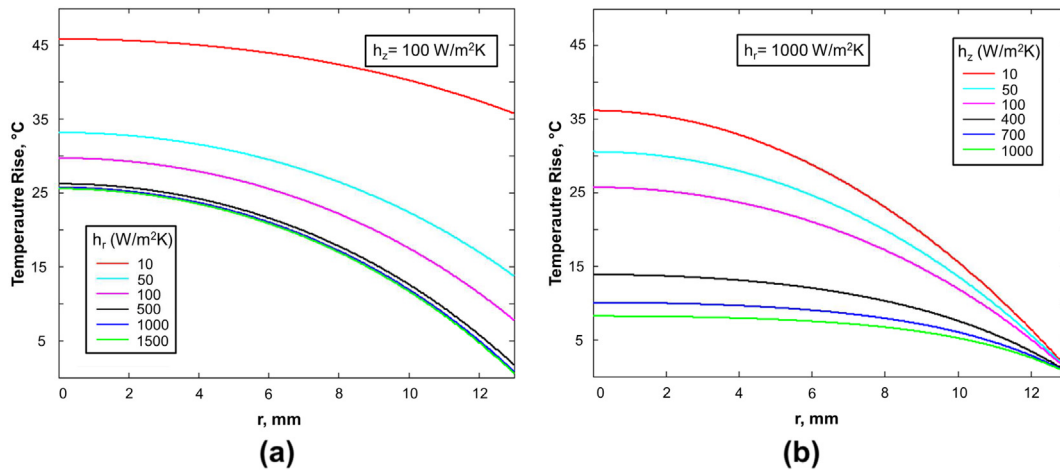
Fig. 6. Temperature as a function of r at mid-height for various values of (a) h_r and (b) h_z.
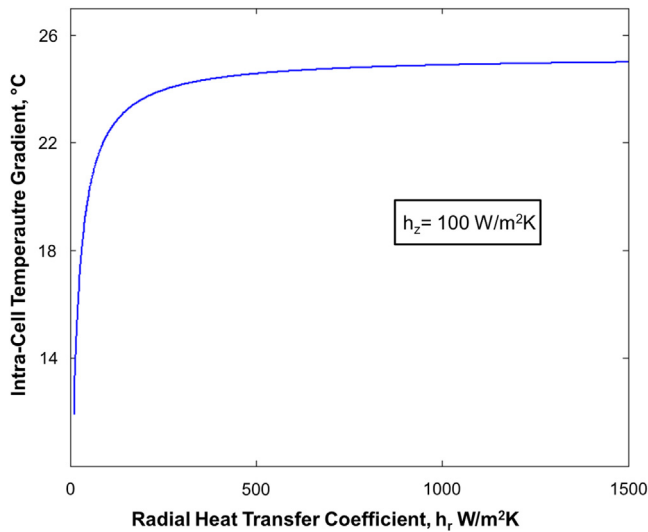

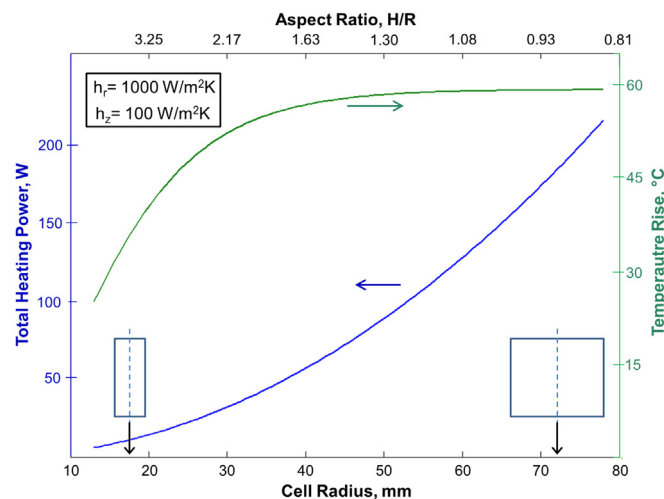**Fig. 7.** Effect of radial heat transfer coefficient on intra-cell temperature gradient.

rise. The increase in temperature with increasing radius however is not as rapid particularly for larger cells because a larger cell has larger outer surface available for convective cooling. Fig. 8 demonstrates the fundamental trade-off between power storage and thermal management. Increasing the cell size makes it more attractive from the power perspective, but also exacerbates the thermal management problem.

While Fig. 8 examines the effect of increasing the cell size, it is also instructive to examine the dependence of peak temperature on the aspect ratio of the cell while maintaining the same total volume. In several applications, the cell volume is fixed due to system-level considerations, while it might be possible to change the aspect ratio within the fixed cell volume. The choice then is whether to have a thin and slender cell, or a short and stout cell. For constant total cell volume V and hence constant total power capacity, the radius and height are related to each other. For a given radius, the height is given by $H = V/\pi R^2$. If convective heat transfer is limited to only the $r = R$ boundary, then assuming uniform heat generation in the cell, the temperature field is given by Equation (15), which shows that the peak temperature at $r = 0$ increases as R increases. Thus in this case, it is thermally preferable to have thin cells of high aspect ratio H/R. If on the other hand, convective heat transfer occurs at both $r = R$ and the top/bottom faces of the cell, then the peak temperature depends on R in a more complicated fashion. Fig. 9
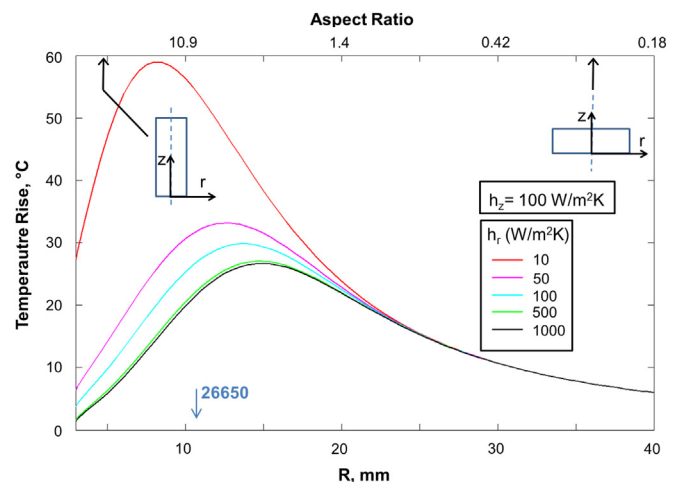

Fig. 8. Effect of battery size on total power and maximum temperature rise, assuming constant power density.

Fig. 9. Variation of peak temperature rise as a function of cell radius and aspect ratio for fixed total cell volume.

plots peak temperature rise for this case as a function of R for fixed total volume, fixed h_z, and for different values of the radial convective heat transfer coefficient, h_r. The total fixed volume is assumed to be that of a 26650 cell. Fig. 9 shows that there is a radius at which the temperature rise attains a maxima. This could be considered a worst-case radius, which roughly corresponds to the radius that minimizes the integral of heat transfer coefficient with respect to area over all surfaces. Note that the worst-case radius is a function of h_r and h_z, and that it becomes larger and larger as h_r increases over h_z. Fig. 9 shows the position of the 26650 cell on the x-axis, indicating that the 26650 geometry is far from optimal particularly for low values of h_r. Reducing the radius of the 26650 cell while increasing height to maintain constant volume may be helpful in reducing the peak temperature rise, particularly when the convective heat transfer coefficient h_r is somewhat low.

6. Conclusions

This paper presents an analytical thermal model for predicting the steady-state temperature field in a cylindrical Li-ion cell. Models with uniform as well as non-uniform heat generation are presented. Experiments are carried out to validate the model, and there is good agreement between the two. Analysis of the dependence of the temperature field on various physical parameters of the problem is presented. It is shown that there is significant potential for temperature reduction by improving radial thermal conductivity and axial convective heat transfer coefficient of the Li-ion cell. Two battery sizing problems of engineering interest are also discussed based on the model presented in the paper. These examples illustrate various design trade-offs between power storage and temperature rise. The analytical models presented in Sections 2 and 3 provide the foundation of thermal design tools for designing safe, high performance Li-ion cells. The analytical models discussed in this paper provide the fundamental foundation on which thermal prediction and optimization for safe, high performance Li-ion cells can be carried out. The capability of fast and accurate temperature prediction of a cylindrical cell may be helpful for rapid iterative design as well as run-time thermal management and control.

References

[1] M. Armand, J.-M. Tarascon, Nature 451 (2008) 652–657.
[2] B. Scrosati, J. Garche, J. Power Sources 9 (2010) 2419–2430.
[3] L. Winkless, Mater. Today 16 (2013) 108.
[4] D. Lisbona, T. Snee, Process Saf. Environ. Protect. 89 (2011) 434–442.
[5] D. Bernardi, E. Pawlikowski, J. Newman, J. Electrochem. Soc. 132 (1985) 5.
[6] K.E. Thomas, J. Newman, J. Power Sources 119 (2003) 844–849.
[7] A.A. Pesaran, M. Keyser, in: Proc. Ann. Battery Conf., 2001.
[8] G.-H. Kim, A. Pesaran, R. Spotnitz, J. Power Sources 170 (2007) 476–489.
[9] Q. Wang, P. Ping, X. Zhao, G. Chu, J. Sun, C. Chen, J. Power Sources 208 (2012) 210–224.
[10] C.Y. Wang, W.B. Gu, B.Y. Liaw, J. Electrochem. Soc. 145 (1998) 3407–3417.
[11] A. Du Pasquier, F. Disma, T. Bowmer, A.S. Gozdz, G. Amatucci, J.M. Tarascon, J. Electrochem. Soc. 145 (1998) 472.
[12] H. Maleki, G. Deng, A. Anani, J. Howard, J. Electrochem. Soc. 146 (1999) 3224–3229.
[13] T.M. Bandhauer, S. Garimella, T. Fuller, J. Electrochem. Soc. 158 (2011) R1–R25.
[14] S.J. Drake, D.A. Wetz, J.K. Ostanek, S.P. Miller, J.M. Heinzel, A. Jain, J. Power Sources 252 (2013) 298–304.
[15] G. Karimi, X. Li, Int. J. Energy Res. 37 (2012) 13–24.
[16] A. Mills, S. Al-Hallaj, J. Power Sources 41 (2005) 307–315.
[17] R. Sabbah, R. Kizilel, J.R. Selman, S. Al-Hallaj, J. Power Sources 182 (2008) 630–638.
[18] T. Bandhauer, Electrochemical-thermal Modeling and Microscale Phase Change for Passive Internal Thermal Management of Lithium Ion Batteries (Ph.D. thesis), Georgia Institute of Technology, 2011.
[19] Y. Chen, J.W. Evans, J. Electrochem. Soc. 140 (1993) 1833–1838.
[20] W. Fang, O.J. Kwon, C.-Y. Wang, Int. J. Energy Res. 34 (2010) 107–115.
[21] C. Forgez, D.V. Do, G. Friedrich, M. Morcrette, C. Delacourt, J. Power Sources 195 (2010) 2961–2968.
[22] S.C. Chen, C.C. Wan, Y.Y. Wang, J. Power Sources 140 (2005) 111–124.
[23] P. Taheri, M. Bahrami, SAE Int. J. Passenger Cars 5 (2012) 164–176.
[24] P. Taheri, M. Yazdanpour, M. Bahrami, J. Power Sources 243 (2013) 280–289.
[25] S.-C. Chen, Y.-Y. Wang, C.-C. Wan, J. Electrochem. Soc. 153 (2006) A637–A648.
[26] N. Ozisik, Heat Conduction, second ed., John Wiley & Sons, 1993.
[27] H.S. Carslaw, J.C. Jaegar, Conduction of Heat in Solids, second ed., Clarendon Press, 1959.
[28] Y. Yener, S. Kakaç, Heat Conduction, fourth ed., Taylor & Francis, 2008.
[29] E. Kreyszig, Advanced Engineering Mathematics, tenth ed., Wiley Inc., 2011.
[30] F.P. Incropera, D.P. Dewitt, Introduction to Heat Transfer, third ed., Wiley Inc., 2006.